Journal of Catalysis **182,** 328–338 (1999)
Article ID jcat.1998.2331, available online at http://www.idealibrary.com on IDEAL®

Gas Oil Hydrodesulfurization and Pyridine Hydrodenitrogenation over NaY-Supported Nickel Sulfide Catalysts: Effect of Ni Loading and Preparation Method

R. Cid,* P. Atanasova,† R. López Cordero,‡ J. M. Palacios,§ and A. López Agudo§,[1]

*Facultad de Ciencias Químicas, Universidad de Concepción, Concepción, Chile; †Department of Chemical and Nuclear Engineering, University of New Mexico, Albuquerque, New Mexico 87131; ‡Centro de Investigaciones del Petróleo, Washington 169, Ciudad de la Habana, Cuba; and §Instituto de Catálisis y Petroleoquímica, CSIC, Campus Universidad Autónoma, Cantoblanco, 28049-Madrid, Spain

Received June 19, 1998; revised October 28, 1998; accepted November 3, 1998

Nickel sulfide catalysts supported on a NaY zeolite with two different metal loadings were prepared by ion exchange and with or without a subsequent NaOH treatment. The catalysts were characterized by number of techniques and measurements, such as X-ray powder diffraction, X-ray photoelectron spectroscopy, temperature-programmed reduction, energy-dispersive X-ray analysis using a scanning electron microscope, ion back-exchange, and acidity determination. The data showed that after sulfidation, nickel is homogeneously distributed for low Ni loadings, while at high Ni loadings nickel is inhomogeneously distributed and partially located outside the zeolite pores. The NaOH pretreatment enhanced the heterogeneity of Ni distribution and its migration to the external surface of the zeolite, particularly for the high-Ni-containing catalyst. Simultaneously, NaOH pretreatment enhanced significantly the degree of nickel sulfidation. The activities of the catalysts for gas oil hydrodesulfurization (HDS) and pyridine hydrodenitrogenation (HDN) were measured simultaneously at high pressure. The results showed that low-Ni-containing catalysts, and particularly the NaOH-treated one, have the highest intrinsic activity for gas oil HDS. This is due to the combined effect of both their better dispersion and better sulfidation of the Ni phase. For pyridine HDN, the more active catalysts were those with higher acid site density, i.e., the ones not treated with NaOH.

INTRODUCTION

Transition metal sulfides supported on zeolites are active for reactions such as hydrodesulfurization (HDS), hydrodenitrogenation (HDN), and aromatic hydrogenation. In addition, they form an important component of the composite catalysts currently used in modern hydrocracking processes (1–3). A knowledge of the surface and catalytic properties of the zeolite-supported transition metal sulfide catalysts is of interest for the development of more complex commercial catalysts which the petroleum refining industry needs for treating heavier feeds and to satisfy the recent environmental regulations and fuel specifications. These needs have therefore stimulated a strong research effort, aimed at the catalytic and structural characterization of transition metal sulfides in zeolites and particularly the Mo, Ni, and NiMo/Y-type zeolite systems [see, e.g., (4–13) and references therein].

Recently, Vasudevan and Fierro, in a review covering various aspects of HDS, summarized recent works on such zeolite catalysts (12). The authors pointed out that an important problem for the application of zeolite-supported transition metal sulfides as HDS catalysts is the difficulty of maintaining the metal phase highly dispersed inside the zeolite. Indeed, in many studies (3–10) it has been demonstrated that after calcination and/or sulfidation only a small part of the metal remains inside the zeolite cages and a large part of the active phase is located outside the zeolite particles. Our recent results on Ni/USY catalysts (5) indicate the possibility of reducing Ni sulfide segregation by forming small clusters of NiO inside the zeolite cavities (14) prior to sulfidation. It is important to examine further whether or not the latter method of activation/sulfidation allows us to obtain better results for the metal sulfide dispersion and consequently for the catalytic activity. The behavior of zeolite-supported metal sulfide catalysts in HDN reactions has hardly been studied, and the results apparently disagree regarding the influence of the acidity on HDN activity (6, 15–17).

In this work, we aimed to investigate if the Ni sulfide dispersion obtained by direct sulfidation of Ni-exchanged NaY zeolite can be improved by previous stabilization of Ni^{2+} ions in the zeolite supercages transforming them into NiO species which are then sulfided. Information regarding the structure of the catalysts in their oxide and sulfided forms was obtained by means of different characterization techniques. Also, HDS and HDN reactions were studied under close-to-commercial conditions.

[1] To whom correspondence should be addressed. Fax: (+34-91) 5854760. E-mail: alagudo@icp.csic.es.

0021-9517/99 $30.00

EXPERIMENTAL

1. Catalyst Preparation

The starting material was a zeolite NaY [Linde, LZ-Y52, $Na_{56}(AlO_2)_{56}(SiO_2)_{136} \cdot 240H_2O$]. Two NiNaY zeolite catalysts containing 1.17 and 3.94 wt% Ni (12 and 40% of Na^+ exchanged by Ni^{2+}, respectively) were prepared by ion exchange of NaY zeolite with aqueous solutions of $Ni(NO_3)_2 \cdot 6H_2O$ at room temperature. After the exchange, the samples were washed with distilled deionized water and then dried overnight in air at 383 K. They are designated Ni(x)Y, x being the weight percentage of Ni determined by atomic absorption spectrometry (AAS) and calculated on the basis of the dry zeolite.

From the dry Ni(x)Y samples two additional catalysts were prepared as follows. Samples of Ni(x)Y were treated with an aqueous solution of NaOH at pH 11 and maintained in stirring for 1 h, followed by washing to pH 7, drying in air at 383 K, and subsequently calcining at 773 K for 4 h. The NaOH-treated samples are denoted as Ni(x)Y-CL.

A HNaY (78% of Na^+ exchanged) zeolite was also prepared from NaY by ion exchange with an aqueous solution of ammonium acetate and used as a reference.

2. Catalyst Characterization

Surface area and micropore volume of calcined catalysts were calculated from the adsorption–desorption isotherms of nitrogen at 77 K on an Micromeritic ASAP-2000 instrument.

X-ray powder diffraction (XRD) for calcined catalysts was carried out in a Seifert 3000 diffractometer using Cu$K\alpha$ radiation.

A Na^+ back-exchange procedure was performed as follows: 1 g of calcined catalyst was treated with 50 cm^3 of 0.05 M sodium acetate at room temperature for 24 h. After the solution was filtered, the filtrate was analyzed for Ni^{2+} and Na^+ ions by AAS.

Temperature-programmed reduction (TPR) experiments were carried out in a conventional TPR apparatus equipped with a thermal conductivity detector (TCD) as follows: 0.200 g of the catalyst was loaded in the TPR reactor and pretreated at 773 K in an air flow of 25 $cm^3\ min^{-1}$ for 2 h. Thereafter, the sample was cooled to room temperature and air flow was replaced by a reductive mixture of 15 vol% H_2 in N_2 (25 $cm^3\ min^{-1}$). The temperature was linearly increased at 10 K min^{-1}. Sulfided samples were sulfided *ex situ* in a mixture of 15 vol% H_2S in H_2 (12 $cm^3\ min^{-1}$) at 670 K for 4 h. Then the samples were flushed with He (20 $cm^3\ min^{-1}$), cooled to room temperature, and transferred into the TPR reactor with minimum exposure to air.

The X-ray photoelectron spectra for the calcined and sulfided catalysts were recorded on a AHIS HSi (Kratos Analytical) spectrometer, working in constant ΔE mode, at a pass energy of 80 eV, using a magnesium anode (Mg$K\alpha$ = 1256.6 eV, 225 W). The peak positions are relative to the binding energy of Si 2p (103.2 eV) and C 1s (284.6 eV). The high-resolution Ni 2p and S 2p peaks were fitted using a commercial least-squares fitting routine with nonlinear Shirley background subtraction (18).

Energy-dispersive X-ray (EDX) analysis was performed using an ISI DS-130 scanning electron microscope equipped with a Kevex Si/Li detector and a Sun SparcStatium-5 system.

The acidity of sulfided catalysts was measured by titration with *n*-butylamine using a potentiometric method (19).

The overall sulfur content for sulfided catalysts was determined by dissolving catalysts in aqua regia to oxidize sulfided species to sulfate. The sulfate was then precipitated with barium perchlorate using an excess of solution. After separation from the solid, the barium left in the solution was analyzed by AAS, and by difference the amount of barium sulfate was determined.

The samples of sulfided catalysts used for the X-ray photoelectron spectroscopy (XPS), SEM-EDX, acidity, and total sulfur analysis measurements were sulfided as described above for TPR, i.e., *ex situ*, and stored under *n*-heptane to avoid contact with air.

3. Catalytic Activity Measurements

The activities of the catalysts for gas oil HDS and pyridine HDN were simultaneously measured in a high-pressure, continuous-flow microreactor under standard conditions: H_2 pressure, 3 MPa; liquid space velocity (LHSV), 8.8 h^{-1}; H_2 (gas)/feed (liquid) ratio, 408 STP l/l; and reaction temperatures, 598, 623 and 648 K. The feedstock was a gas oil containing 1.28 wt% S and enriched with 0.08 wt% N in the form of pyridine. Catalyst samples of 3 g (particle size 0.25–0.42 mm) were diluted with SiC in a volume ratio of 1 : 3, and sulfided *in situ* with a 7 vol% CS_2/gas oil mixture at 2 MPa and 623 K for 2.5 h. Liquid samples were taken at regular intervals, and S and N contents were determined in an Antek sulfur/nitrogen analyzer. From fractional conversion of sulfur and nitrogen, apparent second-order and first-order rate constants, k_{HDS} and k_{HDN}, were calculated (20).

RESULTS

1. Textural Properties, X-ray Diffraction, and Back-Exchange of Ni^{2+} Ions in the Calcined Catalysts

The BET surface area and micropore volume for the parent NaY zeolite were 890 $m^2\ g^{-1}$ and 0.34 $cm^3\ g^{-1}$, respectively. For the oxide samples neither the surface area nor the micropore volume changed significantly with Ni loading or NaOH treatment, indicating that NaOH treatment does not lead to pore blocking.

TABLE 1

XPS Data—Peak Positions and Relative Intensities for the Oxide Catalysts

Oxide catalyst	Ni $2p_{3/2}$	Satellite	$\frac{I(\text{sat})}{I(\text{Ni}\,2p_{3/2})}$	$\frac{I(\text{Ni}\,2p)}{I(\text{Si}\,2p)}$	$\frac{I(\text{Ni}\,3s)}{I(\text{Si}\,2p)}$	$\frac{I(\text{Ni}\,2p)}{I(\text{Ni}\,3s)} \times 10^2$
Ni(1.17)Y	855.8	861.8	1.08	4.40	0.02	2.20
Ni(3.94)Y	855.8	861.6	0.83	3.91	0.02	1.96
Ni(1.17)Y-CL	855.9	862.1	0.88	11.40	0.09	1.27
Ni(3.94)Y-CL	855.0	861.2	0.72	32.71	0.47	0.69

The XRD crystallinity of all catalysts is similar to that of the original NaY zeolite. No peaks different from those of the parent Ni(x)Y catalysts were detected in the XRD patterns of the Ni(x)Y-CL catalysts.

The percentages of Ni^{2+} ions reexchanged by Na^+ ions are as follows: 2.5% for Ni(1.17)Y, 12.7% for Ni(3.94)Y, 0.2% for Ni(1.17)Y-CL, and 0.8% for Ni(3.94)Y-CL. It is evident that the percentages of reexchanged Ni^{2+} ions for NaOH-treated catalysts are an order of magnitude lower compared with those of the untreated ones.

2. *X-ray Photoelectron Spectroscopy*

2.1. Calcined catalysts. In Table 1 are presented the positions of Ni $2p_{3/2}$ peaks and the XPS relative intensity data for the oxide Ni(x)Y and Ni(x)Y-CL catalysts. The position of the Ni $2p_{3/2}$ peak was constant (855.8 eV) for all catalysts in their oxide form, except for Ni(3.94)Y-CL for which the Ni $2p_{3/2}$ peak appeared at lower binding energy, 855.0 eV. The distance between the main Ni $2p_{3/2}$ and its satellite is constant for all samples but there is a change in the ratio of the intensity of the satellite peak versus the main Ni $2p_{3/2}$ peak. It is obvious that the NaOH treatment leads to a decrease in the relative intensity of the satellite peak and this effect is more evident for the zeolite with higher nickel concentration (Table 1).

The position of 855.8 eV for the Ni $2p_{3/2}$ peak corresponds to Ni^{2+} ions exchanged into the zeolite framework reported for NiNaY zeolites (8) and Ni-USY zeolites (21–23). An XPS study of the Ni $2p_{3/2}$ peak positions and satellite intensities of mixed transition metal oxide spinels (24) showed that, when Ni^{2+} ions shift from tetrahedral to octahedral positions, there is a shift of the Ni $2p_{3/2}$ peak toward lower binding energies by ca. 1 eV, and it is accompanied by a 30% decrease in the relative intensity of the satellite peak. It is obvious that such an effect takes place for the NaOH-treated zeolite samples, and that after the NaOH treatment Ni^{2+} ions are located in octahedral positions. The above statement implies that in the dried zeolite a significant portion of the Ni^{2+} ions were located in tetrahedral positions, which is in agreement with the findings of Suzuki *et al.* (25) that the Ni^{2+} ions in the S_{II}, $S_{II'}$ (supercages) and $S_{I'}$ (sodalite) sites of dehydrated NiNaY zeolites are with trigonal-pyramid or tetrahedral coordination. The effect is more evident for the zeolite with higher nickel content, most probably due to a formation of nickel oxide clusters. Additional support for this conclusion is the presence of a second O 1*s* peak at 529.5 eV in the spectrum of the Ni(3.94)Y-CL catalyst, which has a binding energy identical to that of O 1*s* electrons in NiO.

The changes, in both I(Ni $2p$)/I(Si $2p$) and I(Ni $3s$)/I(Si $2p$) ratios, were compared for the catalysts (Table 1). The expected ratios of Ni $3s$/Si $2p$ peaks for monolayer and homogeneous distribution of nickel on the zeolite matrix were calculated using the Kerkhof and Moulijn model (26): 0.027 for the Ni(1.17)Y sample and 0.09 for the Ni(3.94)Y sample. The comparison of these values with the corresponding experimental ones (Table 1) shows that the experimental value is fairly close to the theoretical one for the Ni(1.17)Y sample and lower than the theoretical value for the Ni(3.94)Y sample. These results are an indication that the nickel distribution in the Ni(1.17)Y is uniform, close to a monolayer distribution, and that in the Ni(3.94)Y catalyst there is a formation of Ni-containing clusters (26). The XPS data for the NaOH-treated samples show that the experimental values for I(Ni $3s$)/I(Si $2p$) are significantly higher than the theoretical values, especially for the Ni(3.94)Y-CL catalyst. This is an indication for a nonhomogeneous distribution of nickel species preferentially on the external surface of the zeolite (26). Obviously, the NaOH treatment leads to a diffusion of nickel ions toward the external surface.

The experimental I(Ni $2p$)/I(Si $2p$) ratios provide additional information on the morphology of the catalysts. The fact that the mean free path of Ni $2p_{3/2}$ electrons is two times lower than that of the Ni $3s$ electrons should make the relative intensities I(Ni $2p$)/I(Si $2p$) even more sensitive to the diffusion of nickel ions toward the external surface. However, the change in the I(Ni $2p$)/I(Si $2p$) ratios as a result of the NaOH treatment is less pronounced. This is an indication that most probably a change in the size of the nickel oxide clusters at the surface occurs simultaneously. The effects of diffusion and cluster growth are practically impossible to distinguish quantitatively solely on the basis of the XPS data. However, one can use the changes in I(Ni $2p$)/I(Ni $3s$) as an indication of the changes in nickel oxide cluster size at the surface (Table 1). For both

NaOH-treated zeolites the I(Ni 2p)/I(Ni 3s) ratio is, however, significantly lower, suggesting formation of NiO clusters; the value for Ni(3.94)Y-CL being very close to the experimental I(Ni 2p)/(Ni 3s) ratio for NiO bulk powder. Comparison between the NaOH-treated zeolites suggests that diffusion of the Ni toward the external surface is higher for the Ni(3.94)Y-CL catalyst, but this is accompanied by the formation of larger nickel oxide clusters, e.g., to a significantly decreased dispersion of nickel in the Ni(3.94)Y-CL catalyst.

2.2. Sulfided catalysts. The curve-fitted X-ray photoelectron spectra in Ni 2p and S 2p regions for all catalysts after sulfidation are presented in Figs. 1 and 2, respectively. The shape of the Ni 2p envelope with a satellite peak clearly shows the presence of nonsulfided Ni^{2+} species in the catalysts after sulfidation. Table 2 lists the binding energies of the peaks derived from the curve fit for the Ni $2p_{3/2}$ and S $2p_{3/2}$ peaks. The peaks for Ni $2p_{3/2}$ at 853.2 eV and for S $2p_{3/2}$ at 161.5 eV correspond very closely to the values reported in the literature for nickel sulfides [(27–29) and references therein]. The Ni $2p_{3/2}$ peak at 856.4 eV can be assigned to the presence of nonsulfided Ni^{2+} species in the zeolite framework (21–23). But this binding energy is also

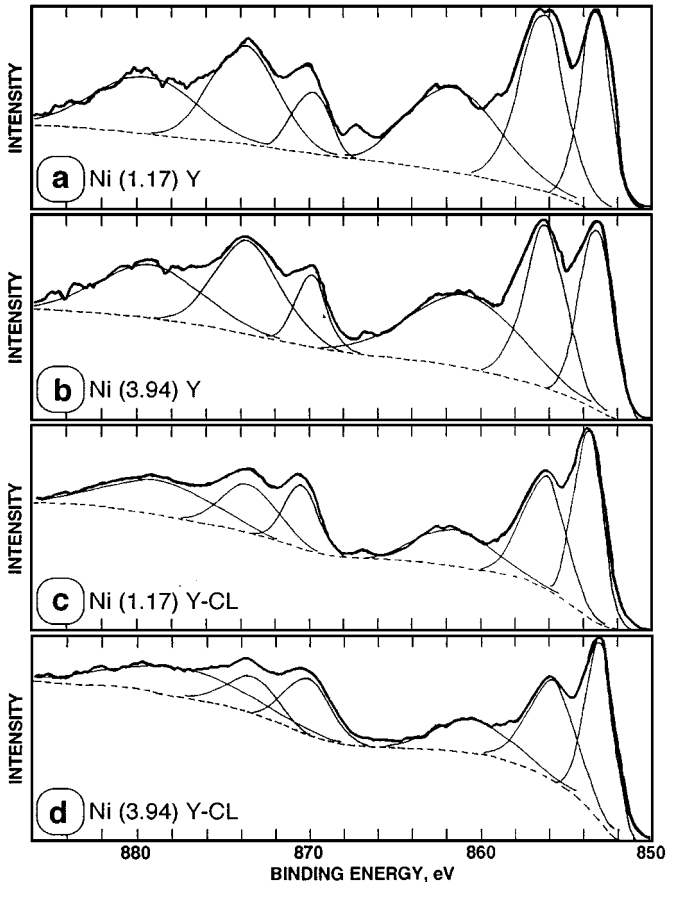

FIG. 1. XPS spectra for sulfided catalysts in the Ni 2p region.

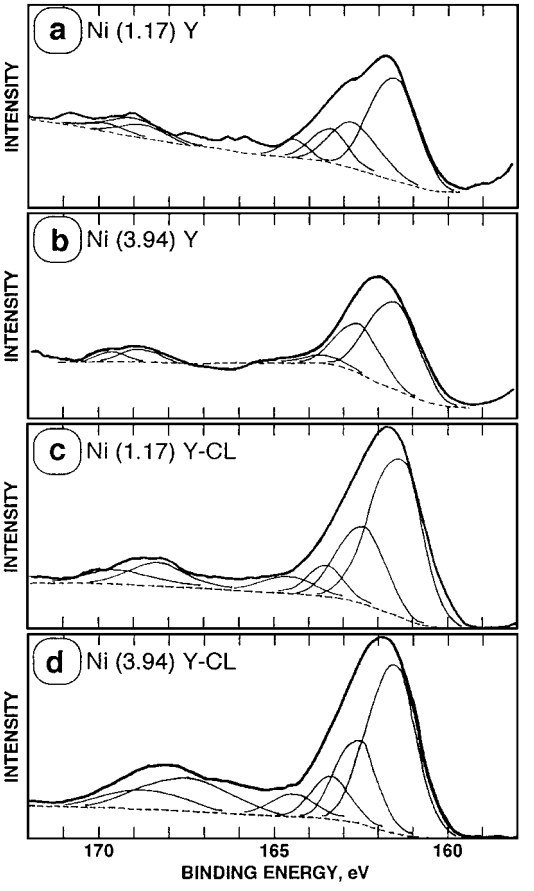

FIG. 2. XPS spectra for sulfided catalysts in the S 2p region.

very close to the Ni $2p_{3/2}$ peak at 856.8 eV for $NiSO_4$ (27, 28, 30) to be exclusively attributed to a remaining oxidic Ni^{2+} species. Simultaneously, a S $2p_{3/2}$ peak at about 168.5 eV appears for all catalysts, which is very close to the S $2p_{3/2}$ peak for a sulfate, observed at 168.7 (29) and 169.2 eV (31). It indicates the possible presence of nickel sulfate formed from the oxidation of nickel sulfide when introducing the samples in the XPS instrument. The S $2p_{3/2}$ peak appearing at 163.4 eV corresponds to elemental sulfur, which has been observed to have a binding energy at 163.7 eV (32).

The comparison between the I(Ni 3s)/I(Si 2p) relative intensities for the oxide (Table 1) and sulfided (Table 2) catalysts show that they are practically identical. As far as the escape depths for Ni 3s and S 2p electrons are the same, this is an indication that no significant change in the overall distribution of the nickel species on sulfidation occurs. However, the I(Ni 2p)/I(Si 2p) and I(Ni 2p)/I(Ni 3s) relative intensities decrease significantly after sulfidation, which indicates a further increase in the cluster size in which nickel is included and/or the presence of sulfur species in the top surface layers.

The changes in sulfur surface concentration I(S 2p)/I(Si 2p) follow, in general, the changes in nickel surface concentration (Table 2). The overall S : Ni atomic ratio, based

TABLE 2

XPS Data for the Sulfided Catalysts

Sulfide catalyst	Ni $2p_{3/2}$	S $2p_{3/2}$	$\frac{I(\text{Ni}\,2p)}{I(\text{Si}\,2p)}$	$\frac{I(\text{Ni}\,3s)}{I(\text{Si}\,2p)}$	$\frac{I(\text{Ni}\,2p)}{I(\text{Ni}\,3s)} \times 10^2$	$\frac{I(\text{S}\,2p)}{I(\text{Si}\,2p)}$
Ni(1.17)Y	853.2	161.5	1.90	0.02	0.95	0.14
	856.4	163.4				
	861.8 (sat.)	169.0				
Ni(3.94)Y	853.3	161.5	2.46	0.02	1.23	0.24
	856.3	163.4				
	861.1 (sat.)	168.9				
Ni(1.17)Y-CL	853.4	161.5	4.51	0.10	0.45	0.90
	856.1	163.6				
	861.4 (sat.)	168.5				
Ni(3.94)Y-CL	853.0	161.6	13.21	0.40	0.33	2.62
	855.8	163.4				
	860.3 (sat.)	167.9				

on the total S 2*p* and total Ni 2*p* intensities, is close to 1 : 2 for both Ni(1.17)Y and Ni(3.94)Y catalysts, and is 1 : 1 for Ni(1.17)Y-CL and 3 : 2 for Ni(3.94)Y-CL catalysts (Table 3). Apparently, this difference in the overall S : Ni ratio is due to a higher surface concentration of total sulfur in the NaOH-treated catalysts. However, it is also important to compare the S : Ni ratios for the species that appear at peak positions related to nickel sulfide. For the Ni(1.17)Y and Ni(3.94)Y catalysts the S : Ni ratio is about 1.5, and for the NaOH-treated catalysts it is about 2.5.

The percentages of sulfided nickel, reoxidized nickel, and remaining oxidic nickel are also presented in Table 3. Since it was not possible to distinguish between Ni^{2+} in $NiSO_4$ and remaining nonsulfided Ni^{2+} based on the Ni 2*p* peak, we used the area for sulfate species to obtain the corresponding amount of the Ni 2*p* peak area as $NiSO_4$, and then subtract it from the total amount of nonsulfided Ni species. The XPS data undoubtedly show that the sulfidation of Ni in NaOH-treated catalysts is significantly higher compared with their nontreated counterparts.

3. Temperature-Programmed Reduction

3.1. Calcined catalysts. Figure 3 shows the TPR of the oxide Ni(*x*)Y and Ni(*x*)Y-CL catalysts. The two catalysts with low Ni content exhibit similar profiles, with a single broad peak with a maximum at about 733 K, which can be attributed to the reduction of Ni^{2+} ions located mostly in the zeolite supercages. The TPR profile of the Ni(3.94)Y catalyst also shows a broad peak at about 763 K with a shoulder at about 810 K, which was attributed to the reduction of Ni^{2+} ions mainly in the supercages. The TPR profile of the Ni(3.94)Y-CL catalyst exhibits a double peak with maxima at 583 and 708 K. The low-temperature peak at 583 K can be attributed to NiO species that are probably located at the external surface of the zeolite (33). Therefore, as a result of NaOH treatment and calcination, part of the nickel migrates from the supercages to the outer surface of the zeolite particles and forms NiO clusters.

3.2. Sulfided catalysts. The TPR profiles for sulfided catalysts are shown in Fig. 4. A common feature of all

TABLE 3

Additional XPS Data for the Sulfided Catalysts

Sulfided catalyst	$(S:Ni)_{at}$ ratio		Ni in NiS (%)	Ni in $NiSO_4$ (%)	Ni in oxidic species (%)	Degree of Ni sulfidation (%)
	Total S and Ni peaks	NiS peaks				
Ni(1.17)Y	0.58 (1 : 2)	1.7 (3 : 2)	23	8	69	31
Ni(3.94)Y	0.39 (1 : 2)	1.4 (3 : 2)	24	9	67	33
Ni(1.17)Y-CL	1.22 (1 : 1)	2.6 (3 : 1)	35	18	47	53
Ni(3.94)Y-CL	1.44 (3 : 2)	2.5 (3 : 1)	38	33	29	71

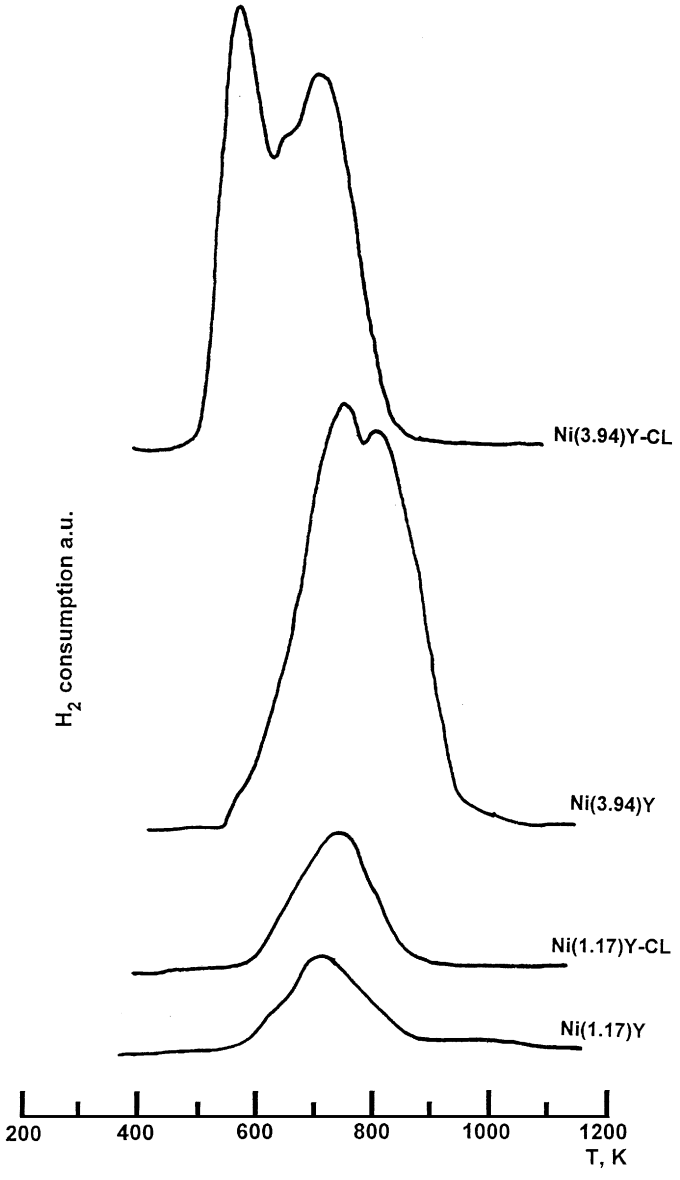

FIG. 3. TPR patterns of oxidic catalysts.

sulfided catalysts is the presence of a sharp peak at very low reduction temperature, with a maximum in the range 510–540 K. The relative intensity of this low-temperature peak increases with NaOH treatment for both low- and high-Ni-containing catalysts. This TPR peak is due either to the reduction of elemental S formed during sulfidation (10) or to the removal of the excess sulfur species associated with transition metals (7, 8) or Na^+ cations of the zeolite (16, 34, 35).

The peak around 700 K observed for the sulfided low-Ni-content catalysts can be attributed to the reduction of nickel sulfide mostly into the supercages. The intensity of this peak is much lower for the NaOH-treated samples. For the Ni(3.94)Y-CL catalyst the peak is apparently shifted to lower temperature (600 K). This shifting can be attributed to reduction of nickel sulfide species segregated outside the zeolite particles. The well-defined high-temperature peak at 880–910 K, which appears for both catalysts with high Ni content, does not seem to be associated with sulfided nickel species. It is possible that it reflects the presence of a small amount of nonsulfided Ni^{2+} species located in sodalite cages or hexagonal prisms, which migrate there during the sulfidation.

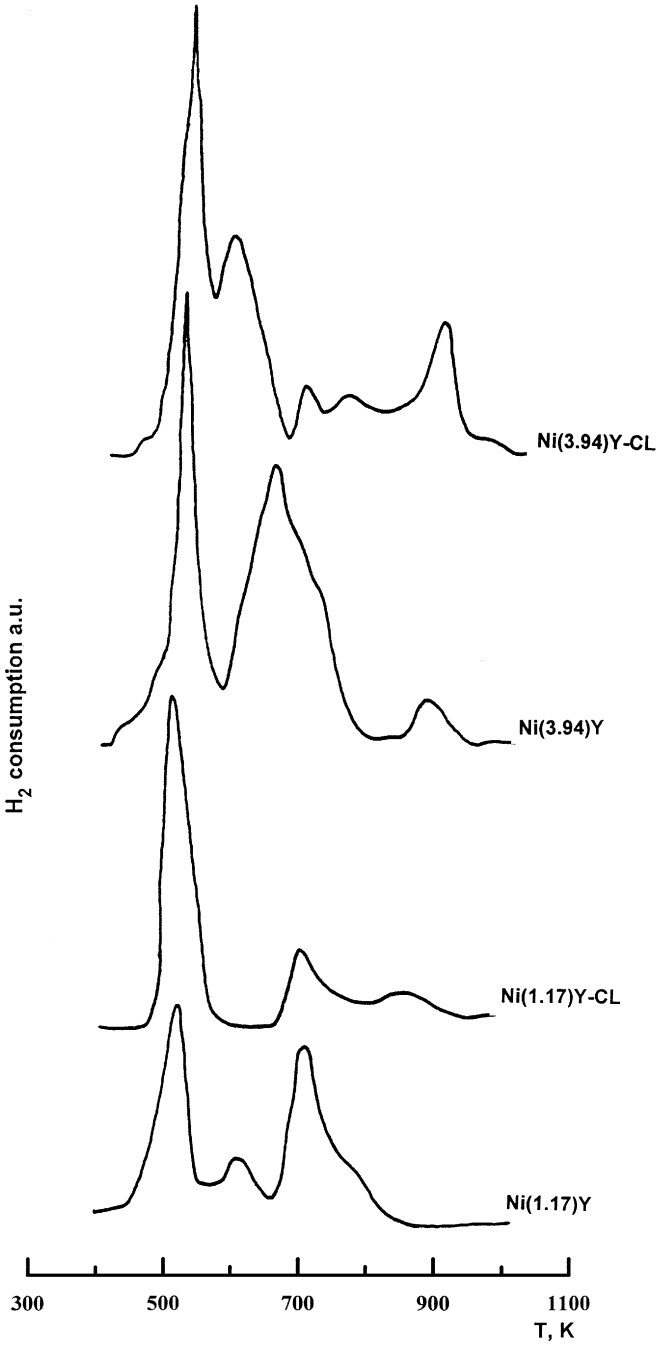

FIG. 4. TPR patterns of sulfided catalysts.

4. EDX and Total Sulfur Analysis

The EDX line profiles of the $K\alpha$ line of Ni across the wafers of the oxide catalysts showed that nickel is evenly distributed in the two low-Ni-content catalysts, inhomogeneously distributed in the Ni(3.94)Y catalyst, and even more inhomogeneous for its NaOH-treated counterpart.

On sulfidation, the EDX spectra in a large zone (ca. 0.5 cm^2) of sulfided Ni(x)Y and Ni(x)Y-CL catalysts revealed that all catalysts have S/Ni ratios higher than that of NiS (used as reference). Table 4 presents the average S/Ni atomic ratios and standard deviations for the EDX spectra of 10 spots randomly selected. The excess sulfur found in all catalysts is due to the presence of elemental sulfur. Formation of elemental sulfur has been observed during sulfidation of transition metal (7, 10)- and alkaline metal (34)-exchanged zeolites. The S/Ni ratio is surprisingly higher (about two times) for the two catalysts with low Ni content compared with the high-Ni-content catalysts, indicating that in the former the formation of elemental S is favored.

Both the S and Ni contents of the sulfided catalysts were chemically analyzed. The results are presented in Table 4. For the Ni(3.94)Y and Ni(3.94)Y-CL catalysts, the S/Ni atomic ratios are higher compared with the Ni_3S_2 phase and very close to the value of NiS, while for the Ni(1.17)Y and Ni(1.17)Y-CL catalysts the S/Ni ratios are even higher than for NiS. Therefore, the low-Ni-containing zeolite catalysts have a significant excess of sulfur, as also found by EDX. This leads us to consider that the formation of an excess of sulfur could be associated with the Na^+ ions of the zeolite. However, when the original NaY zeolite support was subjected to a sulfidation treatment with H_2S/H_2, the chemical analysis did not reveal the presence of sulfur in the NaY zeolite. Thus, the excess sulfur seems to be associated with nickel species, probably those highly dispersed within the zeolite. An excess of sulfur was also reported for sulfided-zeolite-supported Mo (7) and Ni (10) catalysts. This sulfur was considered to be elemental sulfur, which resulted from the sulfidation reaction of NiO to Ni_3S_2 and S (36) or from the combination of various processes in which a dissociation of the H_2S and a partial reduction of Ni^{2+} into Ni^+ were involved (37).

TABLE 4

Average $(S/Ni)_{at}$ Ratio of Sulfided Ni(x)Y and Ni(x)Y-CL Catalysts as Determined by EDX and Total Sulfur Chemical Analysis

Catalyst	$(S/Ni)_{at}$ ratio	
	EDX analysis	Chemical analysis
Ni(1.17)Y	3.2 (0.50)[a]	1.7
Ni(3.94)Y	1.6 (0.06)	1.0
Ni(1.17)Y-CL	3.5 (0.50)	1.9
Ni(3.94)Y-CL	1.6 (0.19)	1.1

[a] In parentheses are the standard deviations (σ) for measurements on 10 small spots.

TABLE 5

Acidity and Intrinsic HDS Activity[a] of Ni(x)Y and Ni(x)Y-CL Catalysts

Catalyst	Total acidity (meq n-butylamine g^{-1})	Acid strength,[b] E_i (mV)	k'_{HDS} (h^{-1} g Ni^{-1})	
			Gas oil HDS	Thiophene HDS
Ni(1.17)Y	1.72	311 (vs)[c]	11.2	6.1
Ni(1.17)Y-CL	1.82	474 (vs)	18.2	14.8
Ni(3.94)Y	1.61	250 (ms)	3.5	3.0
Ni(3.94)Y-CL	1.55	373 (vs)	3.8	3.9
HNaY	2.67	290 (ms)	—	—

[a] Measured at 3 MPa and 623 K.
[b] Estimated by the initial electrode potential, E_i.
[c] vs, very strong; ms, medium strong.

5. Catalyst Acidity

The total acidity of sulfided catalysts as determined by n-butylamine titration is given in Table 5. For the Ni(x)Y catalysts, the number and strength of acid sites increase with increasing nickel loading. This result is expected since for NiY zeolites the acidity generally increases with increasing degree of exchange of Na^+ by Ni^{2+} ions. NaOH treatment of the Ni(x)Y catalysts led to a decrease in their acidity, although the values were still relatively high, due probably to the formation of acidic SH and OH groups during sulfidation (7, 8). The acidic HNaY sample shows, as expected, a large number of acid sites but their strength is lower than for the Ni-containing catalysts.

6. Catalytic Activities

Under the experimental conditions of high pressure used in the present study, the catalysts deactivate slowly with time-on-stream. Their deactivation is much lower than in catalytic tests at atmospheric pressure (5, 8, 10, 11). The catalysts lost between 10 and 15% of their initial activity after 4 h of reaction, and then a steady activity was reached.

In Fig. 5 are shown the gas oil HDS specific activities (per volume of catalyst), k_{HDS}, for the zeolite-supported Ni sulfide catalysts. The Ni(3.94)Y catalyst shows slightly higher HDS specific activity than the Ni(1.17)Y sample. When the catalysts were treated with NaOH, their specific activity was nearly doubled for the low-Ni-content sample and only slightly (about 15%) increased for the high-Ni-content sample. The HDS specific activity of the acidic HNaY zeolite was relatively low, as shown in Fig. 5.

The results of pyridine HDN are shown in Fig. 6. The acidic HNaY zeolite shows the highest pyridine HDN specific activity. In general, all Ni-containing zeolite catalysts

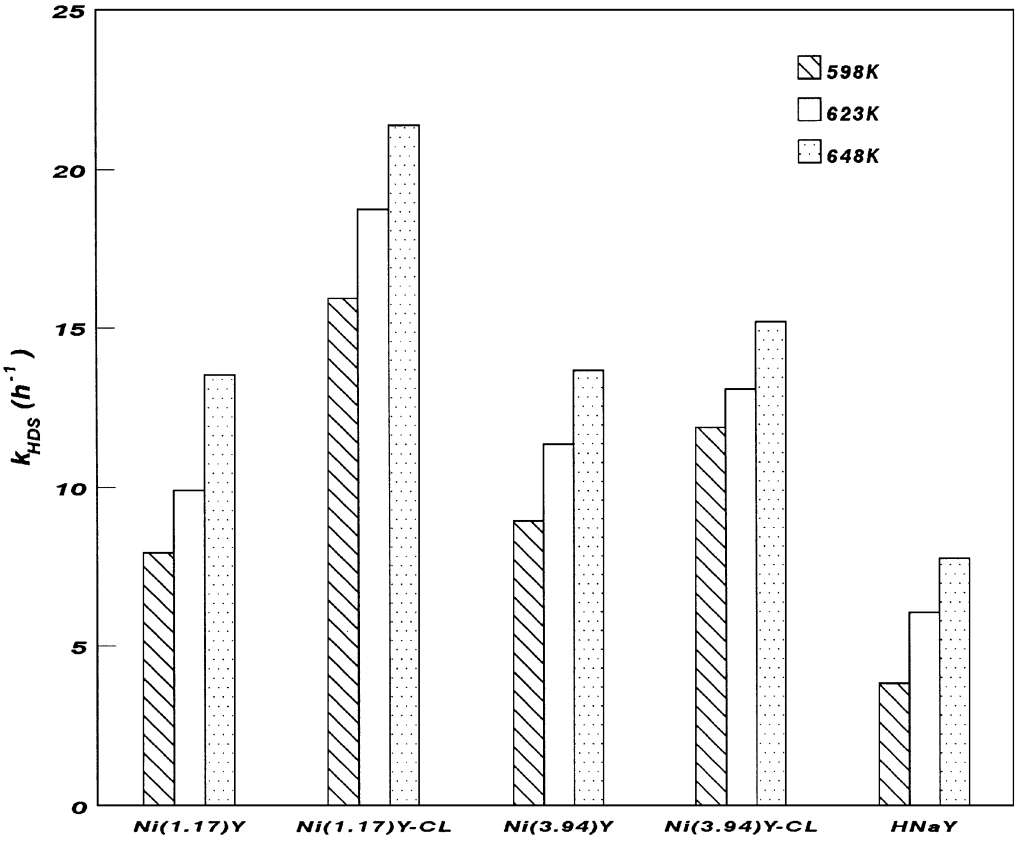

FIG. 5. Specific activities of sulfided catalysts for gas oil HDS in the presence of pyridine.

exhibit lower HDN specific activity, particularly at 598 and 623 K. Similarly to gas oil HDS, for pyridine HDN the Ni(3.94)Y catalyst is slightly more active (per volume of catalyst) than the Ni(1.17)Y catalyst. However, in contrast to HDS, the catalysts treated with NaOH exhibit lower specific activity than their Ni(x)Y counterparts. In particular, Ni(3.94)Y-CL is inactive for pyridine HDN (Fig. 6).

DISCUSSION

1. *Distribution of Ni Species in the Zeolite*

As expected, the distribution of nickel in the calcined Ni(1.17)Y catalyst prepared via Ni^{2+} ion exchange is very homogeneous according to both TPR and EDX results. In this sample nickel is uniformly distributed inside the zeolite particles with close to a monolayer distribution, and only Ni^{2+} ions exchanged into the zeolite cavities are present. In the calcined Ni(3.94)Y catalyst, nickel distribution appears slightly less uniform with possible formation of clusters as suggested by XPS. When Ni(x)Y zeolites were treated with NaOH there was a partial transformation of the Ni^{2+} ions to small clusters or particles of NiO (highly dispersed since no detection by XRD was observed). Simultaneously, migration of nickel to the external surface of the zeolite particles has occurred on calcination. The formation of NiO phase in the Ni (3.94)Y-CL catalyst is clearly shown by the shift of 1 eV Ni $2p_{3/2}$ peak to lower binding energy and the presence of a O 1*s* peak that has a binding energy identical to that of O 1*s* electrons in NiO. The formation of NiO and its localization outside the zeolite particles are supported by the TPR results, which show the appearance of a new peak at 583 K due to easily reducible nickel species. The NaOH-treated samples also have very low values of back-exchange of Ni^{2+} by Na^{+} ions (Table 1). The inhomogeneity is more pronounced for the Ni (3.94)Y-CL catalyst than for the Ni (1.17)Y-CL catalyst, but a small amount of NiO may be present in the Ni(1.17)Y-CL catalyst as suggested by XPS.

During the sulfidation process the oxidic nickel species (Ni^{2+} ions and NiO clusters) supported on NaY zeolite are to some extent transformed into nickel sulfide. In this process the overall distribution of the nickel species over the zeolite surface does not change significantly for most of the catalysts, as is derived from the XPS (Tables 1 and 2). But the observed decrease in the I(Ni 2*p*)/I(Si 2*p*) and I(Ni 2*p*)/I(Ni 3*s*) relative intensities between the oxide and sulfided state suggests further increase in the crystal size of the Ni

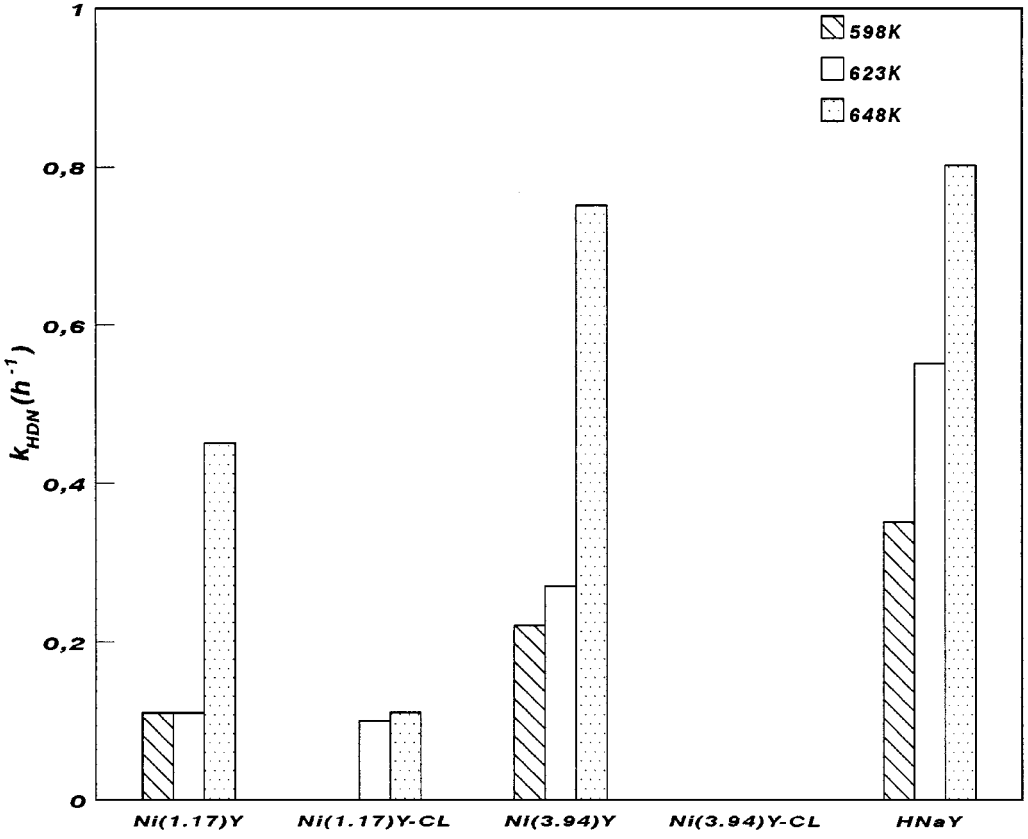

FIG. 6. Specific activities of sulfided catalysts for pyridine HDN measured simultaneously with gas oil HDS.

species during sulfidation. At a bulk level, the TPR results for the low-Ni-content catalysts do not reveal significant changes in the Ni distribution during the sulfidation. However, for the high-Ni-content catalysts the TPR data show that sulfidation causes redistribution of Ni species: part of the Ni migrates further outside the zeolite pores, while a small amount of nonsulfided Ni^{2+} species moves to more internal positions (sodalite or hexagonal prisms) of the zeolite. Thus, in the case of high-Ni-containing catalysts, formation of NiO clusters prior to the sulfidation does not prevent completely the migration of nickel species to the external surface of the zeolite during sulfidation but even facilitates it.

Regarding the extent of sulfidation, the EDX and total sulfur chemical analysis data indicate that the catalysts are completely sulfided because the observed S/Ni ratios are comparable or above the stiochiometric value for the nickel sulfides. However, the XPS spectra (Figs. 1 and 2) and their derived quantitative data (Table 3) clearly show that catalyst sulfidation was incomplete. Relatively large amounts of oxidic Ni^{2+} (30–70%) are still present on sulfidation. The appearance of a high-temperature peak at about 900 K in the TPR of the high-Ni-content sulfided catalysts, attributed to remaining oxidic nickel species located probably in the sodalite or hexagonal prism cages, confirms this.

Furthermore, according the XPS data the extent of sulfidation increases in the order Ni(1.17)Y < Ni(3.94)Y < Ni(1.17)Y-CL < Ni(3.94)Y-CL. The lower extent of nickel sulfidation (~30%) in the Ni(1.17)Y and Ni(3.94)Y catalysts is due to the homogeneous distribution of the Ni^{2+} ions inside the zeolite cavities. The strong interaction of these Ni^{2+} ions with the zeolite framework, especially when they are in the sodalite or hexagonal prism cages, limits their sulfidation. For both NaOH-treated catalysts, it is evident that the formation of NiO clusters facilitates nickel sulfidation (~50 and 70%), especially when they are preferentially located at the outside surface of the zeolite particles.

In the literature, information on the sulfidation behavior of nickel on zeolites varies. Thus, several authors (6, 8, 9, 38) have reported that the sulfidation of nickel on zeolites, after a standard sulfidation procedure, is incomplete. Others (10, 39) have concluded that under such sulfidation conditions the catalysts are fully sulfided. Most probably, the differences in the conclusions are due in part to the use of different characterization techniques to evaluate the degree of sulfidation. In the first case (6, 8, 9, 38) the degree of sulfidation was based exclusively on XPS and IR spectroscopy of adsorbed NO and CO data. In the second case (10, 39) the sulfidation behavior of the catalysts was derived from total sulfur determination by chemical analysis, TPS, EDX

analysis, or gravimetric measurements. However, the latter techniques do not differentiate the oxidation state of sulfur and nickel and if elemental sulfur has been formed during the sulfidation. Consequently, the estimated S/Ni ratio will not reflect the stoichiometry of the nickel sulfide phase only.

As mentioned above, the high S/Ni ratios derived from both EDX and chemical analysis data indicate that an excess of sulfur is present in the catalysts. The excess of sulfur is present either in the form of elemental-like sulfur or as labile nonstoichiometric sulfur. Its presence was confirmed from the low-temperature peak at 510–540 K observed in the TPR of the sulfided catalysts. The presence of elemental-like sulfur at the zeolite surface was also detected, although weakly, by XPS. It is possible that the elemental sulfur was located mainly inside the zeolite cavities or that the labile nonstoichiometric sulfur was removed during the high-vacuum conditions in the XPS instrument. It is also remarkable that the S/Ni XPS ratio corresponding only to the sulfided Ni species is close or higher than 1.5 for all catalysts, a value well above the stoichiometric ratio for bulk NiS and Ni_3S_2. This large excess of surface sulfur could be a nonstoichiometric sulfur strongly chemisorbed on coordinatively unsaturated sites (40), and different from the labile sulfur since it remains after evacuation.

2. *Catalyst Activity*

As shown in Table 5, the intrinsic activity (per gram of Ni) for gas oil HDS decreases in the order Ni(1.17)Y-CL > Ni(1.17)Y $\gg$ Ni(3.94)Y-CL > Ni(3.94)Y. The higher HDS intrinsic activity of the low-Ni-containing catalysts compared with the high-Ni-containing catalysts may be attributed to the more homogeneous distribution of nickel sulfide and its location mainly in the zeolite supercages in the former catalysts. However, both NaOH-treated catalysts exhibit higher HDS activity than their nontreated counterparts, and in the former catalysts the nickel sulfide is more inhomogeneously distributed.

On the other hand, the order of HDS intrinsic activity differs considerably from that of sulfided catalysts acidity. Thus, neither nickel dispersion nor catalyst acidity alone can account for the HDS activity, because both type of sites have ability to catalyze HDS reactions. Most probably, a synergetic effect between the nickel sulfide particles and the acid sites of the zeolite, as proposed by Welters *et al.* (10), occurs. This effect will most likely be present when the metal sulfide particles are located inside the zeolite cages and in close vicinity of the acid sites. However, both Ni(1.17)Y and Ni(3.94)Y catalysts have lower HDS intrinsic activities than their NaOH-treated counterparts. Therefore, the HDS activity should also be influenced by other factors, such as diffusional limitations for the large sulfur compounds in gas oil to enter inside the zeolite cavities and/or differences in the extent of nickel sulfidation.

One way to verify the hypothesis for diffusional limitations is to evaluate the HDS activity with a smaller sulfur compound such as thiophene. In Table 5 the intrinsic activity values (per gram of Ni) for thiophene HDS are compared with those for gas oil HDS. The ranking of the catalysts for both thiophene and gas oil HDS is essentially the same. Therefore, the observed differences in HDS activity among the catalysts cannot be due to diffusional limitations for the large sulfur compounds in the gas oil. The other factor, which may influence the HDS activity, is the degree of nickel sulfidation. The XPS data show (Table 3) that nickel sulfidation was incomplete and reached a different extent for each catalyst. Thus, both NaOH-treated catalysts, when compared with their nontreated counterparts, have a much higher degree of nickel sulfidation (Table 3), which agrees with their higher HDS activity (Fig. 5). The former catalysts have lower nickel sulfide dispersion than the latter catalysts. Obviously, the extent of nickel sulfidation is a factor that more strongly influences the catalyst activity than does dispersion.

If, however, catalysts with a similar degree of nickel sulfidation are compared, i.e., Ni(1.17)Y versus Ni(3.94)Y (~30% nickel sulfidation) and Ni(1.17)Y-CL versus Ni(3.94)Y-CL (above 50% nickel sulfidation), it is obvious that nickel sulfide dispersion becomes of critical importance for HDS activity. In consequence, the HDS activity is determined mainly by nickel sulfide phase dispersion at similar extent of nickel sulfidation in the catalysts, but higher extent of sulfidation (as for the NaOH-treated catalysts) would prevail on the negative effect of lower dispersion.

Regarding HDN activity, comparison of Fig. 6 and Table 5 shows that most active catalysts have higher acid site density, and the NaOH-treated samples, which have lower acid site density, are practically inactive. Thus, under the experimental conditions used, catalyst acidity is the main factor determining HDN activity. The fact that the Ni-free acidic HNaY zeolite exhibited the highest HDN activity suggests that N removal from pyridine in this case could be taking place either by a direct hydrogenolysis enhanced by the presence of H_2S, or by an alternative hydrogenation by hydrogen transfer.

CONCLUSIONS

Low- and high-Ni-content exchanged zeolites and their corresponding NaOH-treated samples were used as precursors for preparation of NaY-supported nickel sulfide catalysts. The NaOH treatment was aimed to improve the Ni sulfide phase dispersion by stabilization of Ni^{2+} through formation of NiO species in the zeolite supercages. It was found that for low-Ni-exchanged NaY zeolite catalysts by this approach, the extent of sulfidation and the gas oil HDS activity were significantly increased. At high level of Ni^{2+} ion exchange the nickel dispersion of the sulfided catalyst

is lower due to a migration of the nickel species outside the zeolite pores, mostly during the calcination process. Thus the phenomenon of migration and sintering was not prevented by transforming the exchanged Ni^{2+} ions into small NiO clusters.

The gas oil HDS activity of the NaY-supported nickel sulfide catalysts was determined by the nickel sulfide dispersion and the extent of nickel sulfidation. The activity of the Ni(x)Y and Ni(x)Y-CL catalysts in pyridine HDN was dominated largely by their acidity.

ACKNOWLEDGMENTS

Financial support from the Scientific Cooperation Program CSIC (Spain)/CONICYT-Fundación Andes (Chile), DGICYT (Spain), and FONDECYT and Dirección de Investigación de la Universidad de Concepción (Chile) is gratefully acknowledged. P. Atanasova is grateful to the Center for Micro-Engineered Materials, University of New Mexico, for financial support. Thanks are also due Mr. Toural Quiroga for assistance in the activity measurements.

REFERENCES

1. Maxwell, I. E., *Catal. Today* **1**, 385 (1987).
2. Yan, T. Y., *Ind. Eng. Chem. Res.* **28**, 1463 (1989).
3. Dufresne, P., Quesada, A., and Mignard, S., *Stud. Surf. Sci. Catal.* **53**, 301 (1990).
4. Leglise, J., Manoli, J. M., Potvin, C., Djega-Mariadassou, G., and Cornet, D., *J. Catal.* **152**, 275 (1995).
5. Cid, R., Neira, J., Godoy, J., Palacios, J. M., and López Agudo, A., *Appl. Catal. A Gen.* **125**, 169 (1995).
6. Arias, P. L., Cambra, J. F., Güemez, M. B., Legarreta, J. A., Pawelec, B., and Fierro, J. L. G., *Bull. Soc. Chim. Belg.* **104**, 197 (1995).
7. Welters, W. J. J., Vorbeck, G., Zandbergen, H. W., van de Ven, L. J. M., van Oers, E. M., de Haan, J. W., de Beer, V. H. J., and van Santen, R. A., *J. Catal.* **161**, 819 (1996).
8. Cid, R., Fierro, J. L. G., and López Agudo, A., *Zeolites* **10**, 95 (1990).
9. Pawelec, B., Fierro, J. L. G., Cambra, J. F., Güemez, B., Duque, F., and Arias, P. L., *Bull. Soc. Chim. Belg.* **100**, 915 (1991).
10. Welters, W. J. J., Vorbeck, G., Zandbergen, H. W., de Haan, J. W., de Beer, V. H. J., and van Santen, R. A., *J. Catal.* **150**, 155 (1994).
11. Welters, W. J. J., van der Waerden, O. H., Zandberger, H. W., de Beer, V. H. J., and van Santen, R. A., *Ind. Eng. Chem. Res.* **34**, 1156 (1995).
12. Vasudevan, P. T., and Fierro, J. L. G., *Catal. Rev. Sci. Eng.* **38**, 161 (1996).
13. de Bont, P. W., Vissenberg, M. J., Boellaard, E., van Santen, R. A., de Beer, V. H. J., and van der Kraan, A. M., *Bull. Soc. Chim. Belg.* **104**, 205 (1995).
14. Suzuki, M., Tsutsumi, K., Takahashi, H., and Saito, Y., *Zeolites* **8**, 284 (1988).
15. Harvey, T. G., and Pratt, K. C., *Appl. Catal. A Gen.* **146**, 317 (1996).
16. Kougionas, K., Cattenot, M., Zotin, J. L., Portefaix, J. L., and Breysse, M., *Appl. Catal. A Gen.* **124**, 153 (1995).
17. Zotin, J. L., Cattenot, M., Portefaix, J. L., and Breysse, M., *Bull. Soc. Chim. Belg.* **104**, 213 (1995).
18. Briggs, D., and Seah, M. P. (Eds.), "Practical Surface Analysis by Auger and X-ray Photoelectron Spectroscopy." Wiley, New York, 1983.
19. Cid, R., and Pechi, G., *Appl. Catal.* **14**, 15 (1985).
20. Benitez, A., Ramirez, J., Vazquez, A., Acosta, D., and López Agudo, A., *Appl. Catal. A Gen.* **133**, 103 (1995).
21. Tao, L.-X., Zhang, F.-M., and Zheng, L.-B., *React. Kinet. Catal. Lett.* **57**, 99 (1996).
22. Pawelec, B., Daza, L., Fierro, J. L. G., and Anderson, J. A., *Appl. Catal. A Gen.* **145**, 307 (1996).
23. Sano, M., Maruo, T., Yamatera, H., Suzuki, M., and Saito, Y., *J. Am. Chem. Soc.* **109**, 52 (1987).
24. Allen, G. C., Harris, S. J., and Jutson, J. A., *Appl. Surf. Sci.* **37**, 111 (1989).
25. Suzuki, M., Tsutsumi, K., and Takahashi, H., *Zeolites* **2**, 51 (1982).
26. Kerkhof, F. P. J. M., and Moulijn, J. A., *J. Phys. Chem.* **83**, 1612 (1979).
27. Shalvoy, R. B., and Reucroft, P. J., *J. Vac. Sci. Technol.* **16**, 567 (1979).
28. Dickinson, T., Povey, A. F., and Sherwood, P. M. A., *J. Chem. Soc. Faraday Trans. 1* **73**, 332 (1977).
29. Laurent, E., and Delmon, B., *J. Catal.* **146**, 281 (1994).
30. Shalvoy, R. B., Reucroft, P. J., and Davis, B. H., *J. Catal.* **56**, 336 (1979).
31. Limouzin-Maire, Y., *Bull. Soc. Chim. Fr. I*, 340 (1981).
32. Portela, L., Grange, P., and Delmon, B., *J. Catal.* **156**, 243 (1995).
33. Jacobs, P. A., Linart, J. P., Nijs, H., and Uytterhoven, J. B., *J. Chem. Soc. Faraday Trans. 1* **73**, 1745 (1977).
34. Kougionas, V., Cattenot, M., Zotin, J. L., Portefaix, J. L., and Breysse, M., *Appl. Catal. A Gen.* **128**, 153 (1995).
35. Moraweck, B., Bergeret, G., Cattenot, M., Kougionas, V., Geantet, Ch., Portefaix, J. L., Zotin, J. L., and Breysse, M., *J. Catal.* **165**, 45 (1997).
36. Scheffer, B., Dekker, N. J. J., Mangnus, P. J., and Moulijn, J. A., *J. Catal.* **121**, 31 (1990).
37. Cornet, D., Ezzamarty, A., and Hemidy, J. F., *in* "Proceedings, Vth International Conference on Zeolites" (D. Olson and A. Bisio, Eds.), p. 377. Butterworths, Guilford, 1983.
38. Leglise, J., Janin, A., Lavelley, J. C., and Cornet, D., *J. Catal.* **114**, 388 (1988).
39. Ezzamarty, A., Catherine, E., Cornet, D., Hemidy, J. F., Janin, A., Lavalley, J. C., and Leglise, J., *in* "Zeolites: Facts, Figures, Future" (P. A. Jacobs and R. A. van Santen, Eds.), Studies in Surface Science and Catalysis, Vol. 49, p. 1025. Elsevier, Amsterdam, 1989.
40. Mangnus, P. J., Riezebos, A., van Langeveld, A. D., and Moulijn, J. A., *J. Catal.* **151**, 178 (1995).